J Polym Res (2016) 23:134
DOI 10.1007/s10965-016-1025-2

ORIGINAL PAPER

Crosslinked carboxylated SBR composites reinforced with chitin nanocrystals

Liubo Ma[1] · **Mingxian Liu**[1] · **Qi Peng**[1] · **Yongwang Liu**[1] · **Binghong Luo**[1] · **Changren Zhou**[1]

Received: 20 March 2016 / Accepted: 10 June 2016

Abstract This study aims to develop and characterize the nanocomposites using sulfur cross-linked carboxylated styrene-butadiene rubbers (S-xSBR) as the matrix and chitin nanocrystals (CNCs) as nanofillers. The composites' morphology and properties were examined by light transmittances, fourier transform infrared spectroscopy (FTIR), scanning electron microscope (SEM), X-ray diffraction (XRD), dynamic mechanical analysis (DMA), thermo gravimetric analyzer (TGA), and tensile properties determination. The addition of CNCs has slight effect on transparency of the composite films. FTIR data confirm the interfacial interactions between CNCs and S-xSBR via hydrogen bonds. CNCs are uniformly dispersed in the matrix from SEM result. The addition of CNCs can significantly improve the tensile strength and modulus both in static and dynamic states. The tensile modulus and tensile strength of S-xSBR/CNCs composites with the 4 wt.% CNCs is 62.5 % and 97.6 % higher than that of pure S-xSBR. The storage modulus, glass transition temperature, and the thermal stability of the composites are higher than those of the neat S-xSBR. The mechanical properties of the composite films are water-responsive, as the swollen samples exhibit obviously decreased strength and modulus. The greatest mechanical contrast is shown in the S-xSBR/CNCs composites with 2 wt.% CNCs loading whose tensile modulus decrease from 60.4 to 6.1 MPa after swelling equilibrium. The significant reinforcement effect of CNCs on S-xSBR is attributed to the unique structure of CNCs and the interfacial interactions in the composite.

✉ Mingxian Liu
liumx@jnu.edu.cn

[1] Department of Materials Science and Engineering, Jinan University, Guangzhou 510632, People's Republic of China

Keywords Chitin nanocrystal · Rubber · Composite · Mechanical property

Introduction

Artificial polymer composite materials are broadly applied in many fields to meet the light-weight and high-strength property requirements. Among the used reinforcing materials, polysaccharide nanocrystals (nanowhisker), such as cellulose [1, 2], starch [3–5], and chitin nanocrystals [6–12], show great potential to improve the polymer's mechanical properties, thermal stability, and solvent responsibility without significant affecting the transparency. Many studies have shown that incorporating a small amount (1–10 %) of these nanocrystals into polymers can induce vast improvement in properties [1, 13]. The properties enhancement can be realized by uniform dispersion of the nanocrystals in polymer matrix via solution mixing or melt mixing [14]. In these composite systems, interfacial interactions between the matrix and the filler are critical.

Chitin is a linear polysaccharide which consists of β-(1–4)-linked units of linked units of N-acetyl-2-amino-2-deoxy-D-glucose. It is the second most abundant natural polysaccharide in the world, while the main source of chitin is marine crustaceans like shrimps and crabs [15]. The amorphous domains of chitin can be removed under certain conditions such as acidolysis, and the crystalline domains with whisker-like fibrils can be isolated in nanoscale [16]. Due to the high mechanical properties, easy availability, nontoxicity, biodegradability, low density, and easy modification, the prepared chitin nanocrystals (CNCs) are employed as reinforcing nanofillers for polymers [6–12, 14, 17]. Aqueous suspensions of the CNCs can be prepared by vigorous mechanical shearing or ultrasonic treatment process. CNCs in the aqueous suspension

Published online: 22 June 2016

are typically a few hundred nm long and 15 nm in diameter. The CNCs-polymer composite can be obtained by mixing the CNCs suspension with polymer solution, resulting in film or hydrogel composite [17, 18]. The mixture of CNCs suspension and chitosan or polyvinyl alcohol (PVA) solutions can also be spinned into fibrous mats for wound dressing application [9, 11]. Surface chemical modification of CNCs to decrease their surface energy can improve the dispersibility/compatibility in organic medium and the polymers. For example, poly(3-hydroxybutyrate-co-3-hydroxyvalerate) (PHBV) grafted CNCs can improve the melt point of PHBV [10]. CNCs can form filler network in polymer matrix via hydrogen-bonded interactions, even when the CNCs volume fraction was only a few percent [19]. The formation of the rigid network leads to a high reinforcing effect on the polymer composites and enhanced water-responsive mechanical properties [12, 20].

Carboxylated styrene butadiene (xSBR) latex is a kind of high-polymer dispersion emulsion polymerized by butadiene, and styrene, etc. As a kind of white thick emulsion in appearance, it has good intermiscibility to padding, large volume of filling, strong viscidity, little foam, and solid coating. It is usually applied as back coating of polypropylene fiber, orlon, and knotted carpet for soft and inflexible feel. Additionally, it also can be reinforced by different nanoparticles [21–25]. Our previous work focused on the influence of CNCs on the preparation and properties of xSBR films without addition of crosslinking agent [12]. The CNCs can significantly improve the mechanical properties of xSBR film without sacrifice of transparency.

The present study is aimed at developing and characterizing sulfur cross-linked composite using xSBR as matrix and CNCs as nanofillers. The S-xSBR/CNCs composites' interfacial interactions, morphology, mechanical properties, and swelling properties were examined by estimation of light transmittances, fourier transform infrared spectroscopy (FTIR), scanning electron microscope (SEM), X-ray diffraction (XRD), dynamic mechanical analysis (DMA), thermo gravimetric analyzer (TGA), and tensile properties determination. Also, the mechanical properties change of the composites after immersing in water is also investigated. The properties improvement of the S-xSBR film is attributed to the uniformly dispersed CNCs and the interfacial interactions of the composites.

Experimental

Materials

Chitin powder (K1262) was procured from Sanland-chem International Inc. and used directly, without further purification. The degree of acetylation (DA) of the chitin was assayed by elemental analysis to be 0.98 %. Carboxylated styrene-butadiene rubber (xSBR) latex was purchased from Guangzhou Juntai Materials Co. Ltd., China with 50 % of solid content. xSBR was a copolymer of styrene, butadiene, and acrylic acid. Hydrochloride acid (HCl) (37 % *w*/w) was analytical purity, which was used without further purification. Cross-linking agent sulfur suspension contained 42.5 % of sulfur and 57.5 % water was obtained from Guangzhou double one latex products Co. Ltd., China. All other chemicals were of analytical grade.

Preparation of chitin nanocrystals (CNCs)

The CNCs was prepared according to the references [6]. Firstly, mixing raw chitin with 3 N HCl at the 30 $mL \bullet g^{-1}$ ratio. Nanocrystal suspensions were prepared by hydrolyzing at 104 °C for 90 min with intense stirring. After acid hydrolysis, the suspensions were diluted with distilled water and centrifuged for 10 min at 4000 rpm. The washing process was repeated for three times to remove the excessive acid and the amorphous phase. Afterwards, the suspensions were transferred to a dialysis bag and dialyzed in running water for 2 h, followed by staying in the distilled water overnight. To separate the chitin microfiber into individual nanofibrils, the suspension was treated with ultrasonic treatment with JY99-IIDN ultrasonic cell disruptor (Ningbo scientz company, China) at 800 W for 1 h.

Preparation of sulfur crosslinked xSBR (S-xSBR)/CNCs composite films

S-xSBR/CNCs composite films were prepared by solution-casting method. The CNCs nano-dispersion with the concentration of 0 ~ 5 wt.% prepared by ultrasonic treatment of freeze-dried CNCs powder. Thereafter, CNCs suspension was added to xSBR latex. According to the 100:2 ratio of latex to sulfur, the sulfur suspension was added to the mixture, followed by adding distilled water to obtain the dispersion with weight of 100 g. The mixture dispersion of xSBR/CNCs with sulfur was stirred mechanically for 6 h and then degassed in vacuum. The dispersion was then cast onto a polytetrafluoroethylene (PTFE) mold and dried in the convection oven. After the solvent was evaporated at 40 °C for 12 h, the mold was placed in the vacuum at 60 °C to solidify the dispersion. Each sample was further sulfurized for 4 h in the convection oven at 150 °C with atmospheric pressure. The obtained S-xSBR/CNCs composite films were stored in desiccator before use.

Characterizations

Light transmittances The light transmittances of S-xSBR/CNCs composite films with ~0.30 mm thickness were measured from 200 to 1000 nm by using a UV-1800 (Shanghai Yoke Instrument Co., Ltd., China) UV-vis spectrophotometer.

Fourier transform infrared spectroscopy (FTIR) The FTIR spectra of neat S-xSBR, CNCs, and S-xSBR/CNCs nanocomposites films were measured using attenuated total reflectance (ATR) model in a NICOLET iS10 FT-IR Spectrometer. Thirty-two consecutive scans were taken and their average was stored. Spectra were taken from 4000 to 400 cm^{-1}. The resolution of the wavenumber was 2 cm^{-1}.

Mechanical properties and water responsive determination The neat S-xSBR and S-xSBR/CNCs composite films were cut into the dumbbell shape with width and thickness of 6 mm × 0.3 mm. Then the samples were stretched at 50 mm/min rates with the SHIMADZU AG-1 machine, and then each stress-strain curve was recorded. The data of Young's modulus were automatically given by the TRAPEZIUMX software in the strain range of 0.1 to 0.4 %. Modules at 100 % or 300 % strain of the sample were the stress required to stretch the sample to 100 % or 300 % elongation (strain). To determine the water response to mechanical property of S-xSBR/CNCs composites, the samples were immersed into 50 mL water for 3 days under room temperature. After that, the samples were tested with the same procedure immediately. Besides, the wet samples were re-dried for 6 h at 40 °C in the oven to determine the recovery of S-xSBR/CNCs composites' mechanical property. At least five samples were tested for every sample for reliable data.

Differential scanning calorimetry (DSC) DSC experiment of S-xSBR and S-xSBR/CNCs composites was determined with a Q20 analyzer (TA instrument). The experiment was conducted at a temperature range of −90 to 100 °C with heating rate of 10 °C/min, under a nitrogen atmosphere. The flow rate of nitrogen was 50 mL/min.

Dynamic mechanical analysis (DMA) The dynamic mechanical analyses of S-xSBR and S-xSBR/CNCs composites were determined with a TA Q800 at the oscillation frequency of 1.0 Hz and the heating rate of 3 °C/min. The experiment was conducted in the tensile mode at temperature range of −100 to 100 °C under a nitrogen atmosphere.

Thermo gravimetric analyzer (TGA) The S-xSBR and S-xSBR/CNCs nanocomposites were implemented using TGA thermal analyzer (Mettler-Toledo TGA/DSC3+). The analysis was conducted with temperature program from 30 to 600 °C in a 20 mL/min flow of highly pure nitrogen gas at a heating rate of 10 K/min. Before the measurement, the samples were dried at 70 °C for 24 h to remove the absorbed water.

X-ray diffraction (XRD) XRD profiles of the CNCs, S-xSBR and S-xSBR/CNCs composite films were obtained by using X-ray diffraction (Rigaku, Miniflex600, CuKα, Japan) at the voltage of 40 kV and the current of 40 mA. The scanning angle was from 5^{o} to 60^{o}.

Scanning electron microscopy (SEM) The cross section of the cryofractured surface of the composites films was plated with a thin layer of gold before the observations. The SEM observations were done using a ZEISS, Ultra55 SEM machine at 3.0 kV.

Swelling behavior in water and toluene The degree of swelling of neat S-xSBR and S-xSBR/CNCs composites was determined by measuring the weight of samples immersing in deionized water at room temperature for 3 days. The swelling ratios were calculated according to the following formula.

$$\text{swelling ratio} = \frac{\text{mass of wet sample-mass of dry sample}}{\text{mass of dry sample}} \times 100\%$$

The degree of swelling of neat S-xSBR and S-xSBR/CNCs composites was further determined by measuring the weight of samples in toluene. The samples were cut into the same size thin disks and first weighted (M_0). Then they were immersed in toluene for 3 days at room temperature. Subsequently, they were dried for 12 h at 60 °C and weighted again (M_0'). The relative weight loss (RWL) was calculated according to the following formula.

$$\text{Relative weight loss(RWL)} = \frac{M_0 - M_0'}{M_0} \times 100\%$$

Results and discussion

Appearance and the interfacial interactions of S-xSBR/CNCs composites

Using the solution casting method, S-xSBR/CNCs composites with 0 ~ 5 wt.% content of CNCs was successfully prepared. The appearance of neat S-xSBR/CNCs is shown in Fig. 1(a). It can be seen that the color of the S-xSBR/CNCs composites is blown and darker than unsulfurized composites [12]. They are transparent and their films thickness is about 300 μm. The light transmittances determined by UV-Vis spectrophotometer is shown in Fig. 1(b). The light transmittances the sulfur cross-linked composites is in 33.7 ~ 39.8 %. In addition, the light transmittances of crosslinked composites are slightly decreased due to the addition of CNCs. This is attributed to that the CNCs can increase light refraction and reflection of composite film [26]. With the increase in CNCs loading, the transparency of the composite film slightly decreases. In the visible light wavelength range of 400 ~ 760 mm, the maximum reduction value of the sulfurized composites is 6.6 % compared with pure S-xSBR film. The nano-dispersion of the fillers was obtained by ultrasonic

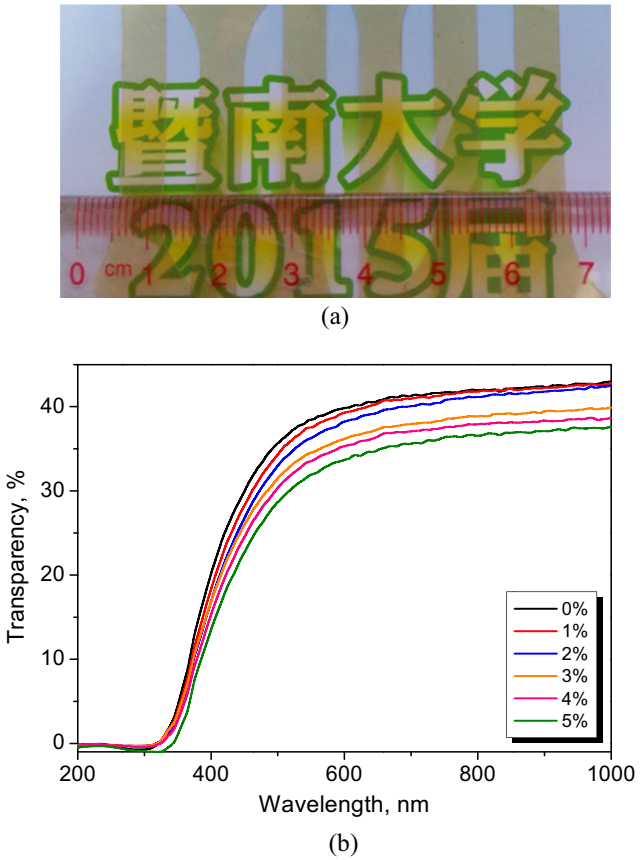

Fig. 1 Appearance (**a**) (From left to right: 0 %; 1 %; 2 %; 3 %; 4 %; 5 %) and the UV—vis light transmittances (**b**) of S-xSBR/CNCs composites

treatment of the CNCs suspensions, appearing highly homogeneous dispersion. The S-xSBR/CNCs composites were obtained by mixing and drying the nano-dispersion of fillers with the xSBR. None aggregated CNCs can be observed in the composite films with naked eyes. The homogeneous dispersion of CNCs is beneficial to the improvement of mechanical and thermal properties of S-xSBR/CNCs composites, which will be illustrated below.

The interfacial interactions between filler and the polymer matrix are critical to influence the composite performance. Theoretically, carboxyl groups on the xSBR can interact with the amide and hydroxyl groups of CNCs via hydrogen bonds. FTIR spectra of CNCs, S-xSBR, and S-xSBR/CNCs (weight ratio, 1:1) were compared to confirm the interfacial interactions (Fig. 2). CNCs show characteristic bands at 3450 cm^{-1} (hydrogen-bonded OH groups), 3264 cm^{-1} (N-H groups), 1660 cm^{-1} (amide I), 1623 cm^{-1} (amide I), and 1554 cm^{-1} (amide II) [27]. S-xSBR show characteristic bands at 3386 cm^{-1} (O-H stretching), 1733 cm^{-1} (carboxyl group), 964 cm^{-1} (1,4 trans butadiene units), 906 cm^{-1} (1,2 vinyl), 752 cm^{-1} (1,4 cis), and 701 cm^{-1} (styrene units) [28]. In the S-xSBR/CNCs composites, the 1660 cm^{-1} and 1623 cm^{-1} peak assigned to amide I shifts to lower wavenumber of 1658 cm^{-1} and 1616 cm^{-1}. The shift is attributed to the hydrogen bonding

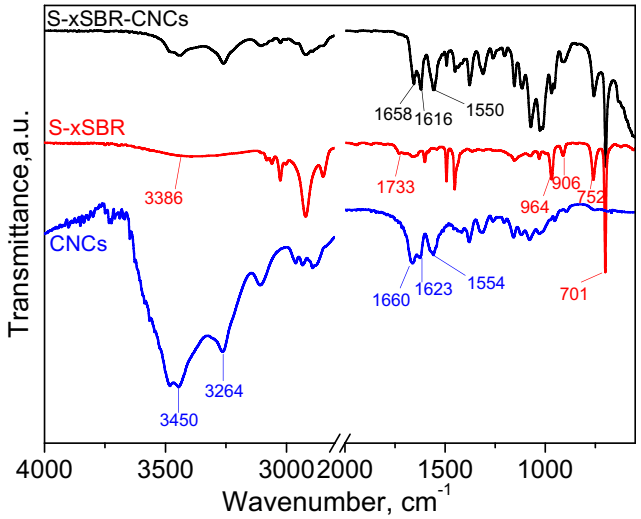

Fig. 2 FTIR spectra of S-xSBR, CNCs, and S-xSBR/CNCs model compound

interactions between the amide and hydroxyl groups of CNCs and the carboxyl group of S-xSBR. Also, the amide II band (1554 cm^{-1}) of CNCs shifts to lower wavenumber of 1550 cm^{-1} in the composite. So, FTIR data confirm the interfacial interactions between CNCs and S-xSBR via hydrogen bonds [12]. The interfacial interactions are benefit for the improvement of the composite properties, which will be illustrated in following section.

Microstructure of the S-xSBR/CNCs composites

XRD and SEM were used to characterize the microstructure of the S-xSBR/CNCs composites. As showed in Fig. 3, around 2θ of 19.5°, there is a wide diffraction peak of neat S-xSBR, which indicates the amorphous state of the rubber matrix. CNCs exhibit two strong scattering peaks at around 2θ of

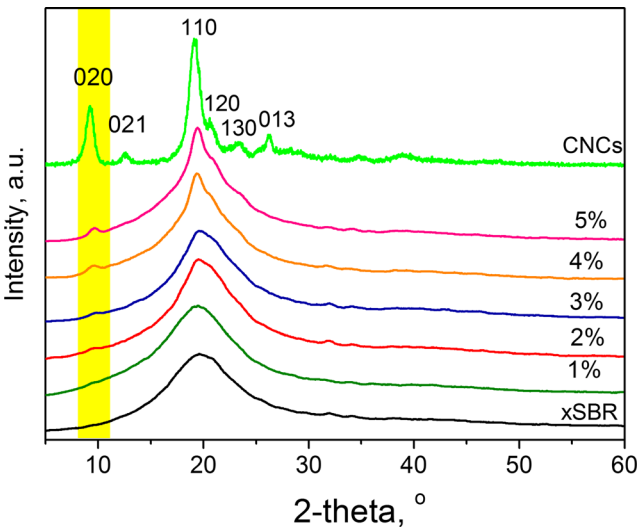

Fig. 3 The XRD patterns of neat S-xSBR and S-xSBR/CNCs composites

9.6° (020 plane) and 19.5° (110 plane) and three other weak peaks at 21° (120 plane), 23° (130 plane) and 26° (013 plane) [27, 29]. No diffraction peak of CNCs can be observed in the composites, until the CNCs content is over 2 wt.%. The peak at 9.6° gradually increases in the S-xSBR/CNCs composites with the increase of CNCs loading, which indicates that CNCs are integrated into the S-xSBR matrix successfully. The (110), (120), and (130) peaks of CNCs in the composites may be overlapped with the peak of the xSBR matrix.

To investigate the dispersion state of CNCs in the S-xSBR, SEM observation was conducted. Figure 4 shows SEM photos of the fracture surface of S-xSBR/CNCs composites. It can be seen that the CNCs (white point with high brightness) are well dispersed in the rubber. The more the CNCs loading is, the more the white points are. No aggregated CNCs is found even when the content reaches 5 wt.%. We also tried to observe the morphology of the composites by transmission electron microscope (TEM). However, no high resolution TEM images can be acquired. This is due to that low atomic number elements (C, O, N, H) of the CNCs result in low contrast between the rubber and the nanocrystals. Nanoscale dispersion of CNCs in the aqueous solution and the composite film can be

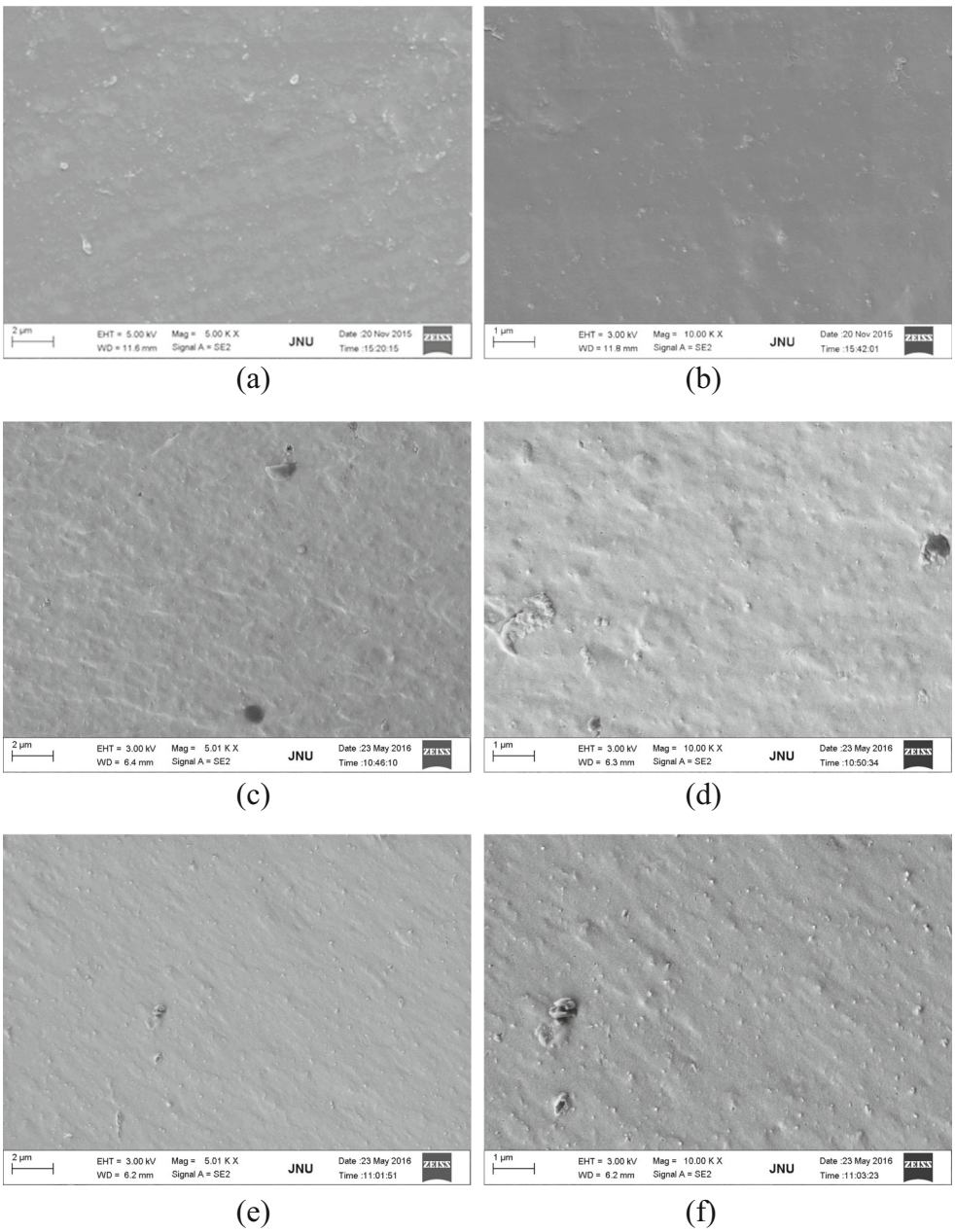

Fig. 4 The SEM photos of the fracture surface of S-xSBR and xSBR/CNCs composites: **a** and **b** S-xSBR; **c** and **d** 1 %; **e** and **f** 2 %; **g** and **h** 3 %; **i** and **j** 4 %; **k** and **l** 5 %

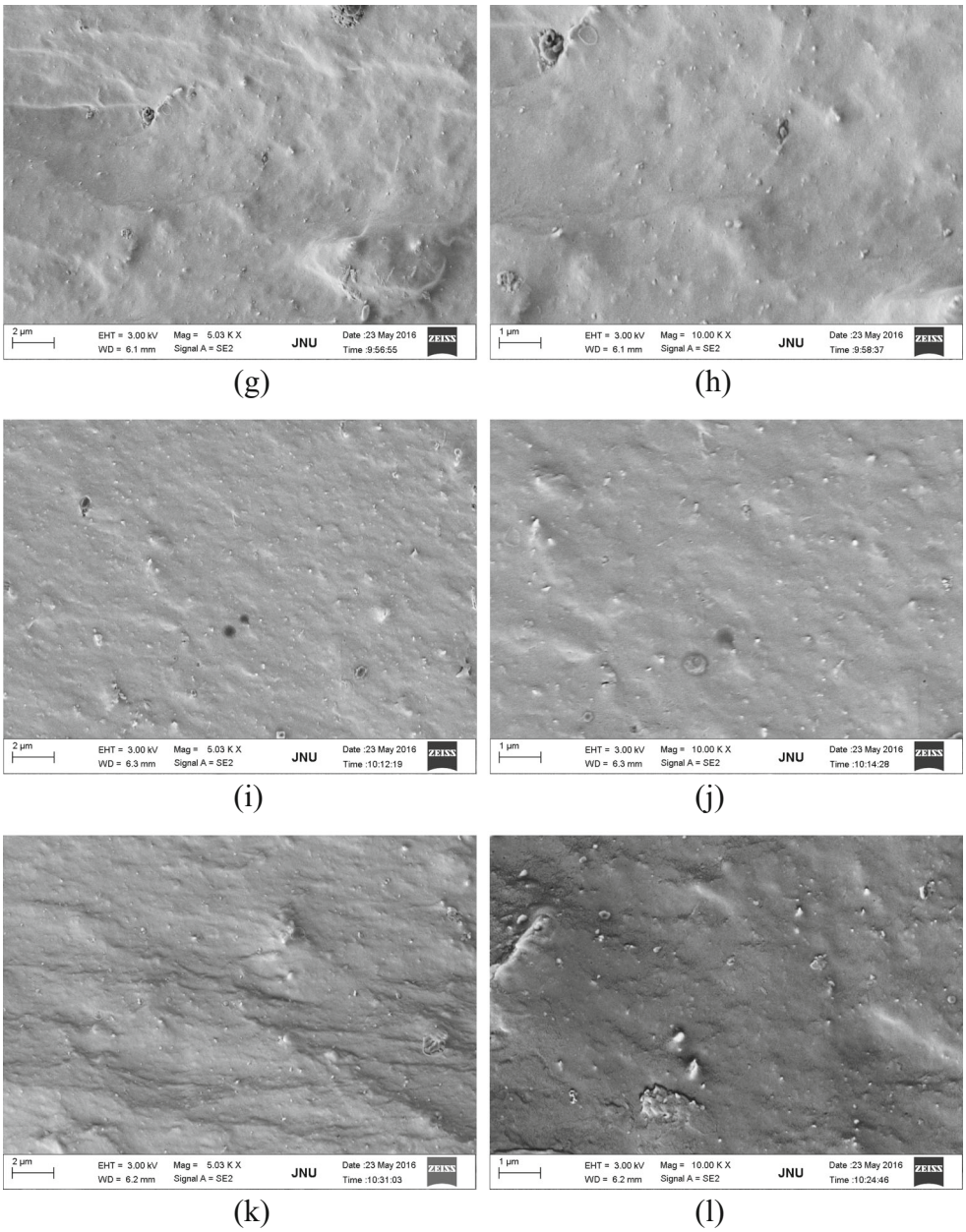

Fig. 4 (continued)

achieved via ultrasonic treatment. The rod-like morphology and charge repulsion effects among CNCs make them possessing a good dispersion capacity. It is significant that the good dispersion state of CNCs endures the stress and heat transfer effectively in the rubber composite. The SEM result is also consistent with the appearance of the materials above.

Mechanical properties of S-xSBR/CNCs composites

The reinforcement of the CNCs on the S-xSBR composite was investigated by the tensile testing. Figure 5(a) shows the typical tensile stress-strain curves for the S-xSBR/CNCs composites. Table 1 summarizes the data of mechanical properties for S-xSBR/CNCs composites. With the increase in the loading of CNCs, the tensile modulus of composites increases obviously. The tensile strength also increases with the CNCs loadings lower than 4 wt.%. CNCs has less effect on the elongation of the S-xSBR composite with the addition of CNCs under 4 wt.% CNCs. For example, with the 4 wt.% CNCs, the rupture elongation of S-xSBR/CNCs composites is 361 %, which is 4.3 % lower than those of pure S-xSBR rubber. But the tensile modulus and tensile strength of the composites increase 62.5 % and 97.6 %, respectively. With 5 wt.% CNCs loading, the tensile modulus of the composite is maximum, which is 2.4 % higher than those of 4 wt.%, while the tensile strength and rupture elongation decrease 6.9 % and

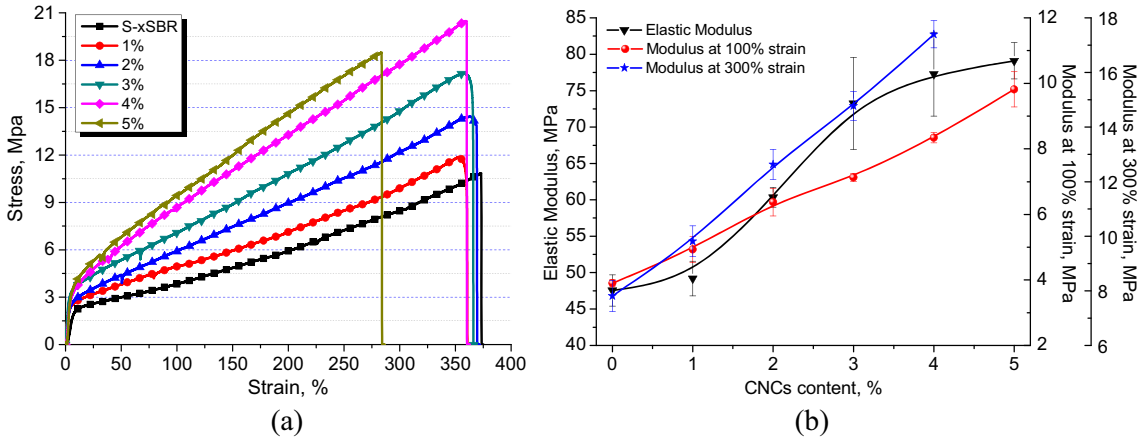

Fig. 5 The tensile stress-strain curves for S-xSBR and S-xSBR/CNCs composites (**a**) and the influence of CNCs loading on the modulus of S-xSBR composites

18.3 % respectively compared with of composites with 4 wt.% CNCs. It seems that overloading of the CNCs cannot induce the sustainable growth of mechanical properties of the composites. Slight amount of CNCs can act as the physical cross linker of the rubber chains and therefore limit the mobility of the polymer chains. CNCs may form a stiff network in the xSBR matrix which can stiffen the composites and suppress the flexibility of the rubber chain. As a result, the elongation at break of the composites decreases when the content of CNCs is high. The elastic modulus, modulus at 100 % strain, and modulus at 300 % strain of the xSBR/CNCs composites increase linearly with CNCs loading (Fig. 5(b)). For example, the S-xSBR composites with 5 wt.% CNCs show the Young's modulus and modulus at 100 % strain of 79.1 MPa and 9.8 MPa, which are 66.3 % and 151.8 % higher than the pure S-xSBR rubber, respectively. The excellent reinforcement effect of CNCs to the xSBR rubber is attributed to the homogeneous dispersion of the rigid CNCs and the hydrogen bonding interactions between the S-xSBR rubber and CNCs [12].

It is also interesting to compare the sulfur crosslinked xSBR/CNCs composites with the unvulcanized xSBR/CNCs composites. As expected, the sulfur crosslinked composites show enhanced strength and modulus. For example, the Young's modulus and tensile strength of the crosslinked xSBR increase 237.3 % and 152.0 %, respectively, compared with the Young's modulus and tensile strength of unvulcanized pure xSBR [12]. It is suggested that the sulfur cross-linking can enhance the macromolecular chain interactions, which result in improved mechanical properties.

Dynamic mechanical and thermal properties of S-xSBR/CNCs composites

The reinforcing effect of CNCs on the S-xSBR composites can be further investigated by the dynamic mechanical analysis. The temperature dependence of the storage modulus (E') and the loss tangent (tan δ) is shown in Fig. 6. Table 2 summarized the value of E' and tan δ value of S-xSBR/CNCs composites. In the rubbery region, the E' of S-xSBR/CNCs composites increases with the loading of CNCs. CNCs filler networks can cause effective load transfer from soft rubber matrix to the rigid fillers. Due to the weak mobility capacity of molecular chains, reinforcement of CNCs on S-xSBR is relatively low in the glassy state.

The T_g of all the materials determined by the DMA is in the range of 22.8 ~ 25.6 °C (Fig. 6(b)), suggesting that CNCs has

Table 1 The mechanical properties for S-xSBR/CNCs composites (The data in the bracket are the standard deviation)

CNCs content (phr)	Young's modulus (MPa)	Modulus at 100 % strain (MPa)	Modulus at 300 % strain (MPa)	Tensile Strength (MPa)	Elongation at break (%)
0	47.56(2.15)	3.90(0.11)	7.82(0.57)	10.81(0.60)	377.4(32.0)
1	49.19(2.37)	4.93(0.40)	9.81(0.57)	11.78(0.53)	368.1(37.2)
2	60.35(1.36)	6.37(0.42)	12.63(0.55)	14.88(0.41)	371.5(29.3)
3	73.25(6.33)	7.13(0.12)	14.78(0.54)	16.52(0.55)	369.7(33.6)
4	77.27(5.76)	8.34(0.16)	17.40(0.54)	21.36(0.48)	361.0(38.5)
5	79.09(2.49)	9.82(0.53)	-	19.89(0.50)	294.8(38.6)

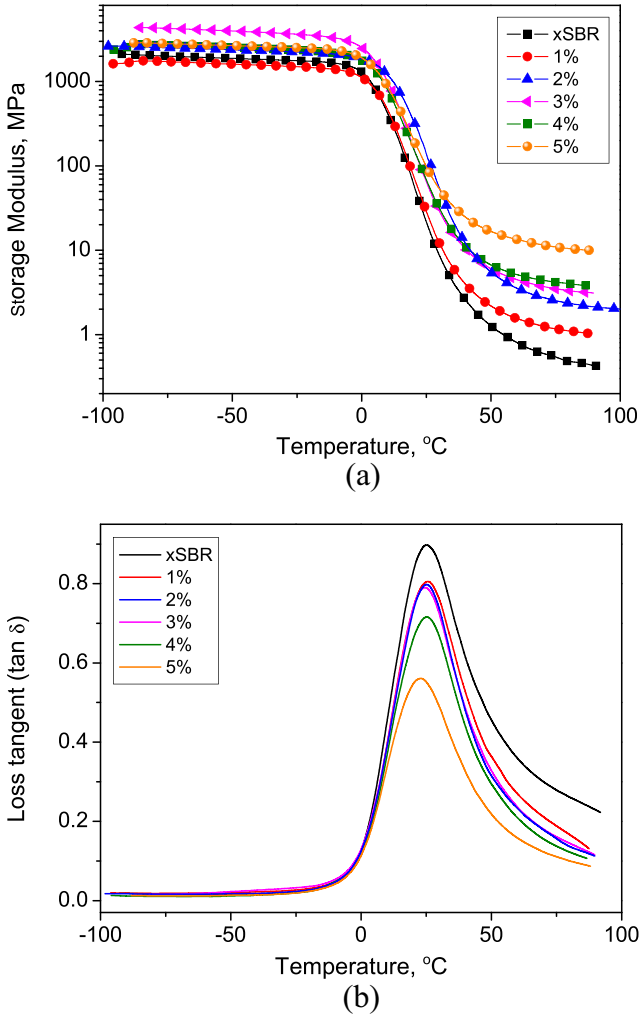

Fig. 6 The temperature dependence of the storage modulus (E') (**a**) and the loss tangent (tan δ) (**b**) for S-xSBR/CNCs composites with various CNCs contents

nearly no significant effect on the glass transition of the S-xSBR. Peak values of tan δ curve decrease with the increase of CNCs. For example, when the loading of CNCs is 5 wt.%, the peak value decreases from 0.90 to 0.56. This is due to the decrease of polymer content in the composites. Moreover, rubber chains can be absorbed on the surface of the CNCs, which restricts their flexibility and mobility. Also the formation of CNCs filler networks in S-xSBR rubber matrix also leads to the decrease of the chain mobility. It is hard to directly observe the formation of filler network in polymer matrix. However, from the tensile mechanical properties result and DMA measurement result of the composites in the present work, it is safe to draw a conclusion of the formation of rigid CNCs network in the S-xSBR matrix. The CNCs can form filler network via hydrogen bonding interactions [20, 21], and therefore, exhibit excellent reinforcing effect on the S-xSBR.

DSC curves of S-xSBR/CNCs composites are shown in Fig. 7(a). T_g of all the materials is in the range of 11.7 to 12.7 °C. Different from the DMA result, DSC method shows the addition of CNCs leads to a slight increase in T_g, although the increase trend is not linearly. T_g obtained from DSC is ~12 °C lower than that from DMA. Difference in T_g values obtained from DMA and DSC arises from the fact that T_g from DMA is highly dependent on the test frequency and variations in the T_g values are possible [30, 31]. The influence of the polymer glass transition temperature by nanofillers depends on the polymer type, filler loading, filler size, filler geometry, filler–polymer interfacial interaction, testing method, testing condition, and so on [32]. Although the rod-like CNCs may form stiff network in the rubber matrix, they do not necessarily showing significant effect on the T_g. This can be understood by the fact that the small size (~15 nm in diameter and ~10 of aspect ratio) and low content of CNCs in the rubber composite.

The influence of the CNCs loading on the thermal stability of the composites was further evaluated by TGA. As seen from Fig. 7(b), the weight loss curve of neat S-xSBR is above the curve of all the S-xSBR/CNCs composites before 475 °C. This is attributed to that the hydrophilic CNCs in the composites leads to more weight loss at relatively low temperature region due to the water loss. However, the composites show higher thermal stability than S-xSBR after 475 °C. This is due to the interfacial interactions between CNCs and xSBR facilitate the improvement of the thermal stability of polymer [31]. Also, all the composites have higher residue than S-xSBR at 600 °C, although the increasing trend is not linearly with the CNCs loading. The TGA result further confirms the

Table 2 The data of storage modulus and loss tangent (tan δ) for S-xSBR/CNCs composites

CNCs content (phr)	Storage modulus at -100 °C (MPa)	Storage modulus at 30 °C (MPa)	Storage modulus at 80 °C (MPa)	tan δ peak values (−)	tan δ peak temperature (°C)
0	2116.2	8.0	0.5	0.90	24.7
1	1625.8	12.1	1.1	0.81	25.5
2	2632.6	52.6	2.3	0.80	24.6
3	4367.7	28.3	3.3	0.79	24.4
4	2386.9	31.1	4.0	0.72	25.6
5	2870.2	50.4	10.5	0.56	22.8

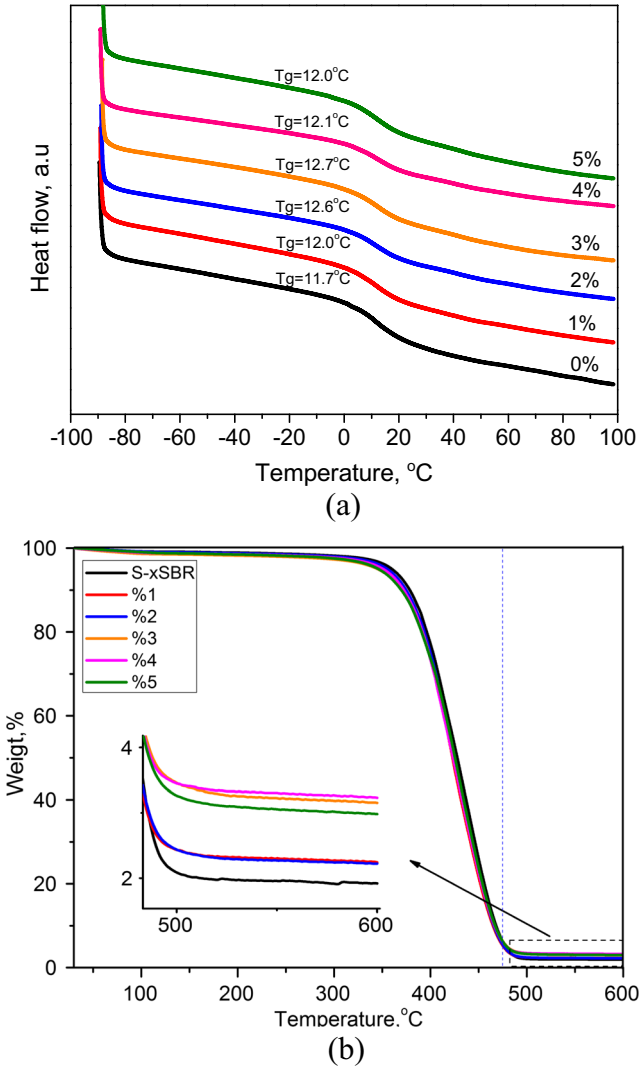

Fig. 7 DSC heating curves (**a**) and TGA curves (**b**) of S-xSBR/CNCs composites with various CNCs contents

successful preparation of the S-xSBR/CNCs composites. The addition of CNCs can improve the thermal stability of S-xSBR/CNCs composites at high temperature region (475 ~ 600 °C). Similar result has also found in the graphene/poly(vinyl chloride) composite [18].

Water response of the mechanical properties of the S-xSBR/CNCs composites

The formation of filler network can influence the swelling behavior of the polymer composite. We investigated the influence of the CNCs on the swelling properties of the S-xSBR by measuring the change of the modulus in wet and dry state. Figure 8 shows the mechanical property of S-xSBR/CNCs composites in the dry state, water-swollen state, and redrying state after swelling. Table 3 compares the modulus change of S-xSBR/CNCs composites before and after swelling. It is clear that the Young's modulus increase with the loading of CNCs. For example, the Young's modulus of S-xSBR/CNCs composites with 5 wt.% CNCs is 79.1 MPa which is 0.66-fold compared with neat S-xSBR. This is attributed to the formation of rigid filler network in the SBR matrix. The modulus at 100 % strain of the composites also increases linearly. The modulus at 100 % strain of S-xSBR/CNCs composites with the 5 wt.% CNCs is 9.82 MPa which is 1.52-fold compared with neat S-xSBR (3.90 MPa). CNCs have an excellent reinforcement effect on S-xSBR especially at high filler content.

The tensile test of the neat S-xSBR and S-xSBR/CNCs composites after immersing in deionized water for 3 days was also conducted. The tensile modulus of all swollen samples decreases as shown in Fig. 8(a) and Table 3. Due to the absent of hydrophilic filler network in the rubber matrix, the tensile modulus of the neat S-xSBR changes 958.87 %. The S-xSBR/CNCs composites with 2 wt.% have a greatest mechanical contrast, showing that the tensile modulus decrease from 60.35 to 6.10 MPa after swelling equilibrium. In addition, the tensile strength of the composites with 2 wt.% CNCs decrease from 14.88 to 4.68 MPa. The 100 % strain of the composites also shows a similar trend after redrying (Fig. 8(b)). The 100 % strain of the all the composite can be completely

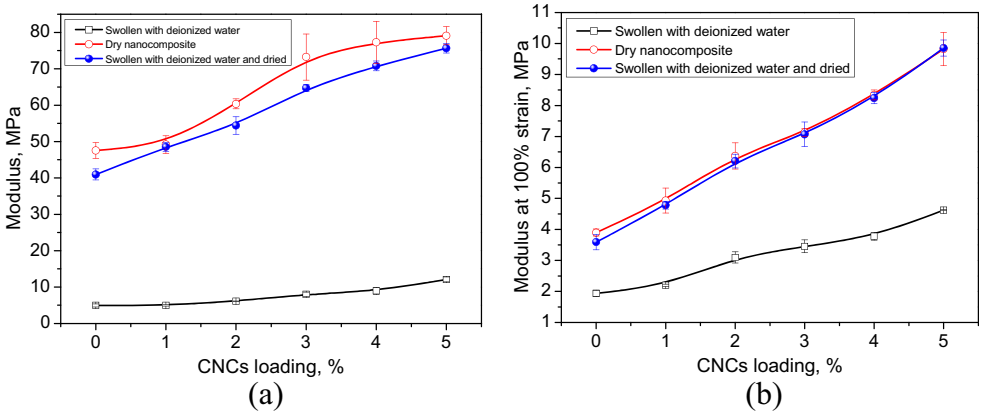

Fig. 8 The tensile moduli of S-xSBR/CNCs composites as a function of CNCs loading in the dry state at 25 °C and water-swollen state (after immersion in deionized water at 37 °C for 5 days). Data points represent averages ($N = 5$) (standard deviation): **a** tensile modulus; **b** stress at 100 % strain

Table 3 The tensile modulus (a) change for S-xSBR/CNCs composites before and after swollen in deionized water (The data in the bracket are the standard deviation)

CNCs content (phr)	Modulus in dry state (MPa)	Modulus in swollen state (MPa)	Change (%)	Modulus of swollen and dried again (MPa)	Recovery ratio (%)
0	47.56(2.15)	4.96(0.43)	958.87	40.95(1.51)	86.10
1	49.19(2.37)	4.99(0.22)	985.77	48.52(1.19)	98.64
2	60.35(1.36)	6.10(0.08)	989.34	54.42(2.38)	90.17
3	73.25(6.33)	8.00(0.59)	915.63	64.70(0.88)	88.33
4	77.27(5.76)	8.95(0.98)	863.35	70.79(1.38)	91.61
5	79.09(2.49)	12.10(0.68)	653.64	75.64(1.27)	95.64

recovered. In contrast, the neat S-xSBR has the lowest recovery ratio on the tensile modulus and modulus at 100 % strain. This suggests CNCs network in the rubber matrix not only can enhance the water response ratio of mechanical properties of the S-xSBR, but also improve the mechanical property recovery ratio after redrying.

Swelling properties of S-xSBR/CNCs composites

The swelling properties of S-xSBR/CNCs composites in water and toluene were conducted to further investigate the influence of CNCs on the structure of S-xSBR. Figure 9(a) shows the water uptake ratio of S-xSBR/CNCs composites with various CNCs content. The water uptake ratio of neat S-xSBR rubber is 8.7 %. Due to the hydrophilicity of CNCs, the water uptake ratios of the composite are higher than that of neat S-xSBR. The maximum value of 14.5 % for the water uptake ratios is achieved at the content of CNCs of 3 wt.%. After that, the water uptake ratio of composites slightly decreases when the CNCs content is over 3 wt.%. This can be explained by the rigid continuous filler networks at high CNCs content to suppress the water absorption of the composite. In brief, the addition of hydrophilic CNCs can improve the water uptake ratio of S-xSBR.

Figure 9(b) compares the relative weight loss in toluene of neat S-xSBR and the S-xSBR/CNCs composites. The dissolution parts of the rubber can be recognized as the free uncosslinked rubber chains which can be dissolved in good solvent. It can be found that the relative weight loss (RWL) of all materials is in the range of 7.1 to 7.3 %. The CNCs have little effect on the dissolution of S-xSBR in toluene. Because this experiment was conducted at room temperature without any stirring, the dissolution ratio of the rubber is limited. Also, the cross-linking by sulfur enhances the adhesion force between rubber and CNCs, which also suppress the dissolution of rubber.

Conclusions

Cross-linked S-xSBR/CNCs composites were prepared by using casting and drying method in the presence of sulfur. The addition of CNCs has slight effect on transparency of films. FTIR data confirm the interfacial interactions between CNCs and S-xSBR via hydrogen bonds. CNCs can be uniformly dispersed in the rubber matrix. The tensile test suggests that the CNCs can improve the tensile strength and the modulus of S-xSBR significantly, while the relatively high content of CNCs leads to the decrease of the elongation at break. In rubber state, the storage modulus of composites increases with the CNCs. The incorporation of CNCs leads to slightly increased T_g of S-xSBR from DSC result. The addition of CNCs can improve the thermal stability of S-xSBR/CNCs composites at high temperature region (475 ~ 600 °C). The mechanical properties of S-xSBR/CNCs composites are water responsive. The CNCs enhance the change ratio of mechanical properties of S-xSBR after swollen in water, but also improve their mechanical recovery after redrying. The CNCs can

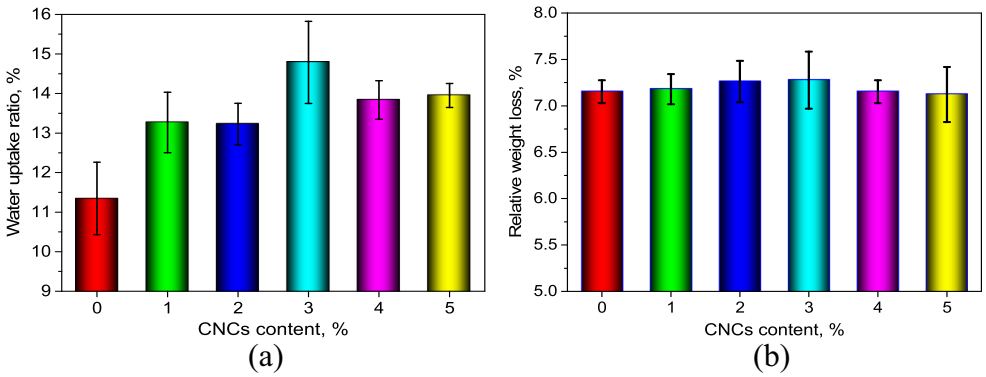

Fig. 9 Water uptake ratios of S-xSBR/CNCs composites as a function of CNCs content (**a**); RWL of S-xSBR/CNCs composites as a function of CNCs content (**b**)

improve the water uptake of S-xSBR, but their loading hardly affects the solution of S-xSBR in toluene. All results suggest the S-xSBR/CNCs composites have enhanced mechanical properties and the composites show promising applications in extensive areas.

Acknowledgments This work was financially supported by National High Technology Research and Development Program of China (2015AA020915), the National Natural Science Foundation of China (grant No. 51473069, 51502113, and 31570981), and the Guangdong Natural Science Funds for Distinguished Young Scholar (grant No. S2013050014606), Science and Technology Program of Guangzhou, China (No. 201510010135), Pearl River S&T Nova Program of Guangzhou (201610010026), and the Fundamental Research Funds for the Central Universities (21615204).

References

1. Cao X, Dong H, Li CM (2007) New nanocomposite materials reinforced with flax cellulose nanocrystals in waterborne polyurethane. Biomacromolecules 8(3):899–904
2. Habibi Y, Lucia LA, Rojas OJ (2010) Cellulose nanocrystals: chemistry, self-assembly, and applications. Chem Rev 110(6): 3479–3500
3. Angellier H, Molina-Boisseau S, Dufresne A (2005) Mechanical properties of waxy maize starch nanocrystal reinforced natural rubber. Macromolecules 38(22):9161–9170
4. Angellier H, Putaux JL, Molina-Boisseau S, Dupeyre D, Dufresne A Starch nanocrystal fillers in an acrylic polymer matrix. In: Macromolecular Symposia, 2005. vol 1. Wiley Online Library, pp 95–104
5. Kristo E, Biliaderis CG (2007) Physical properties of starch nanocrystal-reinforced pullulan films. Carbohydr Polym 68(1): 146–158
6. Gopalan Nair K, Dufresne A (2003) Crab shell chitin whisker reinforced natural rubber nanocomposites. 1. Processing and swelling behavior. Biomacromolecules 4(3):657–665
7. Paillet M, Dufresne A (2001) Chitin whisker reinforced thermoplastic nanocomposites. Macromolecules 34(19):6527–6530
8. Araki J, Yamanaka Y, Ohkawa K (2012) Chitin-chitosan nanocomposite gels: reinforcement of chitosan hydrogels with rod-like chitin nanowhiskers. Polym J 44(7):713–717
9. Uddin AJ, Fujie M, Sembo S, Gotoh Y (2012) Outstanding reinforcing effect of highly oriented chitin whiskers in PVA nanocomposites. Carbohydr Polym 87(1):799–805
10. Wang J, Wang Z, Li J, Wang B, Liu J, Chen P, Miao M, Gu Q (2012) Chitin nanocrystals grafted with poly (3-hydroxybutyrate-co-3-hydroxyvalerate) and their effects on thermal behavior of PHBV. Carbohydr Polym 87(1):784–789
11. Naseri N, Algan C, Jacobs V, John M, Oksman K, Mathew AP (2014) Electrospun chitosan-based nanocomposite mats reinforced with chitin nanocrystals for wound dressing. Carbohydr Polym 109: 7–15
12. Liu M, Peng Q, Luo B, Zhou C (2015) The improvement of mechanical performance and water-response of carboxylated SBR by chitin nanocrystals. Eur Polym J 68:190–206
13. Grunert M, Winter WT (2002) Nanocomposites of cellulose acetate butyrate reinforced with cellulose nanocrystals. J Polym Environ 10(1–2):27–30
14. Zeng J-B, He Y-S, Li S-L, Wang Y-Z (2011) Chitin whiskers: an overview. Biomacromolecules 13(1):1–11
15. Rinaudo M (2006) Chitin and chitosan: properties and applications. Prog Polym Sci 31(7):603–632
16. Marchessault RH, Morehead FF, Walter NM (1959) Liquid Crystal Systems from Fibrillar polysaccharides. Nature 184(4686):632–633
17. Liu M, Huang J, Luo B, Zhou C (2015) Tough and highly stretchable polyacrylamide nanocomposite hydrogels with chitin nanocrystals. Int J Biol Macromol 78:23–31
18. Huang Y, Yao M, Zheng X, Liang X, Su X, Zhang Y, Lu A, Zhang L (2015) Effects of chitin whiskers on physical properties and osteoblast culture of alginate based nanocomposite hydrogels. Biomacromolecules 16(11):3499–3507
19. Capadona JR, Shanmuganathan K, Tyler DJ, Rowan SJ, Weder C (2008) Stimuli-responsive polymer nanocomposites inspired by the sea cucumber dermis. Science 319(5868):1370–1374
20. Dagnon KL, Shanmuganathan K, Weder C, Rowan SJ (2012) Water-triggered modulus changes of cellulose nanofiber nanocomposites with hydrophobic polymer matrices. Macromolecules 45(11):4707–4715
21. Florjanczyk Z, Debowski M, Wolak A, Malesa M, Plecha J (2007) Dispersions of organically modified boehmite particles and a carboxylated styrene-butadiene latix: a simple way to nanocomposites. J Appl Polym Sci 105(1):80–88
22. Cao X, Xu C, Liu Y, Chen Y (2013) Preparation and properties of carboxylated styrene-butadiene rubber/cellulose nanocrystals composites. Carbohydr Polym 92(1):69–76
23. Abdollahi M, Rahmatpour A, Khanli HH (2007) Structure and mechanical properties of carboxylated styrene-butadiene rubber (XSBR)/pristine clay nanocomposites. E-Polymers 7(1): 1753–1760b
24. Alimardani M, Abbassi-Sourki F, Bakhshandeh GR (2012) Preparation and characterization of carboxylated styrene butadiene rubber (XSBR)/multiwall carbon nanotubes (MWCNTs) nanocomposites. Iran Polym J 21(11):809–820
25. Du M, Guo B, Lei Y, Liu M, Jia D (2008) Carboxylated butadiene–styrene rubber/halloysite nanotube nanocomposites: interfacial interaction and performance. Polymer 49(22):4871–4876
26. Lu Y, Sun Q, She X, Xia Y, Liu Y, Li J, Yang D (2013) Fabrication and characterisation of α-chitin nanofibers and highly transparent chitin films by pulsed ultrasonication. Carbohydr Polym 98(2): 1497–1504
27. Goodrich JD, Winter WT (2007) A-chitin nanocrystals prepared from shrimp shells and their specific surface area measurement. Biomacromolecules 8(1):252–257
28. De Sarkar M, De P, Bhowmick A (2000) Diimide reduction of carboxylated styrene–butadiene rubber in latex stage. Polymer 41(3):907–915
29. Cho Y-W, Jang J, Park CR, Ko S-W (2000) Preparation and solubility in acid and water of partially deacetylated chitins. Biomacromolecules 1(4):609–614
30. Haines PJ (2002) Principles of thermal analysis and calorimetry. Royal society of chemistry, London
31. Vadukumpully S, Paul J, Mahanta N, Valiyaveettil S (2011) Flexible conductive graphene/poly (vinyl chloride) composite thin films with high mechanical strength and thermal stability. Carbon 49(1):198–205
32. Jordan J, Jacob KI, Tannenbaum R, Sharaf MA, Jasiuk I (2005) Experimental trends in polymer nanocomposites—a review. Mater Sci Eng A 393(1):1–11